The Journal of Chemical Physics

Dehydration induced dynamical heterogeneity and ordering mechanism of lipid bilayers

Cite as: J. Chem. Phys. **154**, 174904 (2021); https://doi.org/10.1063/5.0044614
Submitted: 18 January 2021 . Accepted: 08 April 2021 . Published Online: 03 May 2021

Sheeba Malik, and Ananya Debnath

The Journal of Chemical Physics ARTICLE scitation.org/journal/jcp

Dehydration induced dynamical heterogeneity and ordering mechanism of lipid bilayers

Cite as: J. Chem. Phys. 154, 174904 (2021); doi: 10.1063/5.0044614
Submitted: 18 January 2021 • Accepted: 8 April 2021 •
Published Online: 3 May 2021

Sheeba Malik and Ananya Debnath[a)]

AFFILIATIONS

Department of Chemistry, Indian Institute of Technology Jodhpur, Karwad, Rajasthan, India

Note: This paper is part of the JCP Special Collection in Honor of Women in Chemical Physics and Physical Chemistry.
[a)]**Author to whom correspondence should be addressed:** ananya@iitj.ac.in

ABSTRACT

Understanding the influence of dehydration on the membrane structure is crucial to control membrane functionality related to domain formation and cell fusion under anhydrobiosis conditions. To this end, we perform all-atom molecular dynamic simulations of 1,2-dimyristoyl-sn-glycero-3-phosphocholine dimyristoylphosphatidylcholine lipid membranes at different hydration levels at 308 K. As dehydration increases, the lipid area per head group decreases with an increase in bilayer thickness and lipid order parameters indicating bilayer ordering. Concurrently, translational and rotational dynamics of interfacial water (IW) molecules near membranes slow down. On the onset of bilayer ordering, the IW molecules exhibit prominent features of dynamical heterogeneity evident from non-Gaussian parameters and one-dimensional van Hove correlation functions. At a fully hydrated state, diffusion constants (D) of the IW follow a scaling relation, $D \sim \tau_\alpha^{-1}$, where the α relaxation time (τ_α) is obtained from self-intermediate scattering functions. However, upon dehydration, the relation breaks and the D of the IW follows a power law behavior as $D \sim \tau_\alpha^{-0.57}$, showing the signature of glass dynamics. τ_α and hydrogen bond lifetime calculated from intermittent hydrogen bond auto-correlation functions undergo a similar crossover in association with bilayer ordering on dehydration. The bilayer ordering is accompanied with an increase in fraction of caged lipids spanned over the bilayer surface and a decrease in fraction of mobile lipids due to the non-diffusive dynamics. Our analyses reveal that the microscopic mechanism of lipid ordering by dehydration is governed by dynamical heterogeneity. The fundamental understanding from this study can be applied to complex bio-membranes to trap functionally relevant gel-like domains at room temperature.

I. INTRODUCTION

Lipid bilayers are essential components of cell membranes that act as semi-permeable boundaries between extra and intra-cellular environments. Lipid bilayers at fluid phase maintain the functionality of cells at physiological temperature.[1] The fluidity of the membrane is largely controlled by its hydration level or the water contents. Although the primary functions of membranes such as hosting trans-membrane proteins, exchange of bio-molecules for transport, and drug-delivery are relevant at fully hydrated states for most organisms, a broad range of species can live under anhydrobiosis conditions over a long period of time.[2,3] The activity of anhydrous cell membranes in such organisms is important to their ability to avoid dissociation and is of tremendous biological importance.[4] Moreover, understanding biological membranes at low hydration levels are relevant for cryo-preservation techniques with large applications in food science, pharmacology, clinical medicine, and the preservation of human embryos for *in vitro* fertilization.[5,6]

Since water is a key parameter for the function and stability of membranes,[7–9] the macroscopic architecture of membranes changes with the hydration numbers. Upon lowering the water content, phospholipid bilayers undergo a more ordered state.[10] Although water near bio- and soft-surfaces has received much attention in the last decade,[11–17] the physics of water and membrane dynamics correlation and its effect on the structure have not been fully explored yet. Therefore, the present study focuses on understanding the underlying dynamics that causes dehydration-directed fluid-to-gel crossovers of bilayers.[10,15]

Recently, many experimental studies have shown the slowdown of water dynamics at lower hydration numbers near bilayers.[18–26]

Thermodynamics of chain melting phase transition of diacylphosphatidylethanolamines obtained from calorimetric measurements as a function of water content has been studied. The free energy, enthalpy, and entropy of phase transition have a tanh dependence on water content in terms of interlamellar water thickness and correlation length of water order.[27] Frequency modulation atomic force microscopy experiments show the existence of two hydration layers near supported dipalmitoylphosphatidylcholine bilayers.[28] Using the dynamic atomic force microscope technique in association with a carbon nanotube probe, it has been shown that the hydration force and molecular ordering of water can be modified by changing the membrane fluidity.[29] Dynamical experiments have shown columnar order in liquid crystalline phases of stacked lipid bilayers due to the coupling between the two-dimensional intralayer domain growth and interlayer smectic ordering[30] assisted by solvents. Using infrared spectroscopy, an increased fraction of well-structured, low density network water has been observed near the POPC bilayer upon dehydration similar to super-cooled water near −25 °C.[31] Nuclear magnetic resonance (NMR) spectroscopy has shown that the water diffusion near the egg PC-water system, DOPC, and POPC bilayer system depends on the change in the hydration number.[18,19] Using ultrafast polarization selective vibrational spectroscopy, a slowdown in orientational relaxation of water has been observed near artificial multibilayers of the phospholipid dilauroyl phosphatidylcholine DLPC as the hydration of water decreases.[20] Two major types of interfacial water molecules are found: one clathrate-like cluster associated with choline moieties and the hydration water near phosphate groups. Using terahertz spectroscopy, it has been found that the bulk-like water dynamics slowly disappear at a lower hydration level and fast and slow reorienting water molecules appear.[21] Using neutron scattering experiments,[22] the effect of hydration numbers on DMPC bilayers above and below the main phase transition temperature is recorded. Quasi-elastic neutron scattering experiments (QENS)[32] and simulations have been performed for the 1,2-Dipalmitoyl-sn-glycero-3-phosphocholine (DPPC) bilayer at low hydration numbers. It is observed that the melting of the bilayer occurs at higher temperature at lower hydration due to the packing of the bilayer.

Complementary to the experiments, molecular dynamics (MD) simulations have been performed to understand the structural and dynamical properties of water at the microscopic level. The reorientational auto-correlation function (RACF) is calculated to understand the orientation of water molecules near the bilayer surface on varying the hydration number. The water relaxation time increases from high to low water contents.[9,10,33,34] Interfacial water (IW) near the phospholipid bilayer are very strongly bound via hydrogen bonds (HBs) to the polar groups of the lipid bilayer.[33] For DMPC as well as for DOPC bilayers, diffusion of the IW slows down on lowering the hydration number.[9,10] Bilayers become more ordered as the number of water molecules per lipid decreases. The order parameter, area per head group, and thickness of DMPC, DOPC, and POPC bilayers confirm that the fluid phase changes to a gel phase as water per lipid is lowered to ~10. Similar to the slowdown of the IW near the bilayer phase change, the slowdown of the IW are found near dynamical crossovers of proteins or cryoprotecting biomolecules using MD simulations and neutron scattering experiments.[35,36] The changes in the bilayer structure and the slowdown of water dynamics induced by dehydration are clearly observed in previous experiments and simulations. Although the interplay between the water dynamics and the ordering of membranes upon lowering water contents has been investigated in a previous molecular dynamics study,[10] the relation of growing relaxation time scales of interface water with dehydration and its effect on the spatial distributions of the local dynamics of membranes remain unattended so far.

The present study reveals the relation between slow relaxation of the interface water to dynamical heterogeneity when the water content is lowered. The objective of this work is to find out how dehydration induces dynamical heterogeneity in the interface water and how the heterogeneous coupled dynamics of the interface water and the local lipids influences the bilayer ordering. To this end, we have performed all-atom MD simulations at different water contents near dimyristoylphosphatidylcholine (DMPC) bilayers. To understand the dynamical properties of water near the bilayer, translational mean square displacements (MSDs) of IW are calculated for various water contents. A plateau-like behavior in MSD has indicated the emergence of dynamical heterogeneity in IW upon dehydration. To confirm the existence of dynamical heterogeneity upon dehydration, non-Gaussian parameters (NGPs), 1D van-Hove correlation functions, and self-intermediate scattering functions (SISFs) are calculated for the IW. Relations between the diffusion constant and α relaxation times are analyzed at different water contents. The hydrogen bond auto-correlation function and reorientational auto-correlation function (RACF) of IW are calculated. To establish the correlation between dynamical heterogeneity and the bilayer fluid-to-gel crossover, the order parameter, area per lipids, and 2D van Hove correlation functions of bilayers are calculated. Our results show that the dynamical heterogeneity arises in the IW as well as in the bilayer upon lowering the water contents. The emergence of dynamical heterogeneity leads to the chain ordering of the bilayer at room temperature. Thus, this work provides the mechanistic insights into the dehydration induced bilayer ordering.

II. SIMULATION DETAILS

Figure 1(a) shows the structure of a DMPC molecule. An equilibrated configuration of a fully hydrated bilayer with 128 DMPC molecules in the presence of 5743 TIP4P/2005[37,38] water molecules is used as the starting configuration [Fig. 1(b)] to generate bilayers with different water contents. CHARMM36[39] force fields are used for DMPC bilayers. CHARMM36 in combination with TIP4P/2005 is known to work well for calculating water dynamics near a membrane at the fluid phase.[38,40,41] The fully hydrated bilayer corresponds to ω = 45, where ω represents the water content or the hydration number. At ω = 45, the bilayer is in the fluid phase, as previously reported in experiments.[20,22,42,43] Figure S1 in the supplementary material shows that the fully hydrated bilayer reaches the diffusive regime confirming the fluid phase. Eight different bilayers are generated from the equilibrated bilayer where ω ranges from 45 to 4 (45, 35, 32, 26, 18, 10, 8, 6 and 4) at 308 K (Table I). Figure 1(c) shows the equilibrated bilayer with ω = 4.

The GROMACS-4.6.5[44–48] software package is used to conduct these simulations.

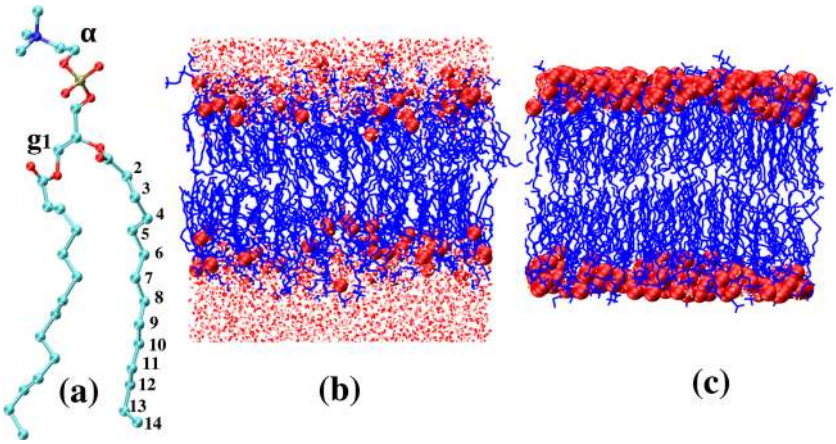

FIG. 1. Snapshot of (a) a DMPC molecule (explicit hydrogen atoms are not shown for the purpose of the clarity). DMPC bilayer for (b) ω = 44 and (c) ω = 4. (Color code with representation) DMPC: CPK (Corey–Pauling–Koltun) representation in blue; water: red; and IW water: VDW (van der Waals) representation in red.

All bilayers in Table I are equilibrated at 308 K temperature using the Berendsen method[49] with a coupling constant of 0.5 ps in NPT ensembles with a time step of 2 fs. Semi-isotropic pressure coupling is applied using the Berendsen method[49] to maintain the pressure of 1 bar with compressibility factors of 4.5×10^{-5} bar^{-1} and coupling constants of 1.0 ps independently in xy and z directions. Here, the changes in the x–y dimensions are independent of the ones along the z axis. A cutoff of 1.2 nm is used for van der Waals interactions. For electrostatic interactions, the particle mesh Ewald approach[14,50,51] is used. Periodic boundary conditions are applied in xyz directions. Thus, the simulated bilayers are multilamellar stack due to the periodic boundary conditions. The LINCS[52] algorithm is used to keep bonds with hydrogen constant. The equilibration period in the NPT ensemble is 550 ns for ω = 45 and 100 ns for remaining systems. System sizes of the equilibrated bilayers are mentioned in Table I. Next, NVT runs are performed for 1 ns with a 0.4 fs time step and a 10 fs saving frequency without constraints for all bilayers. Nose–Hoover temperature coupling is used to maintain the temperature of 308 K with a coupling constant of 0.5 ps. Long- and short-range distance corrections for the NVT runs are the same as for the NPT runs. The center of mass motions are removed during the NVT production runs. Different run-lengths are used for different dynamical calculations to obtain good statistics as such high frequency runs are expensive for the all-atom MD simulations of the bilayers.

Additionally, a bulk water (BW) system consisting of 851 water molecules is simulated using the TIP4P/2005 water model at 308 K to compare water dynamics with dynamics of IW near bilayers with different water contents.

TABLE I. Details of the systems studied.

Hydration number (ω)	Water molecules	Box size (nm)
45	5 743	6.27 × 6.27 × 7.90
35	4 480	6.35 × 6.35 × 6.75
32	4 096	6.34 × 6.34 × 6.49
26	3 328	6.29 × 6.29 × 5.02
18	2 304	6.41 × 6.41 × 5.02
10	1 331	6.22 × 6.22 × 4.69
8	1 024	6.05 × 6.05 × 4.60
6	768	5.92 × 5.92 × 4.57
4	512	5.77 × 5.77 × 4.56
45	51 687	18.27 × 18.27 × 7.90
4	4 608	17.37 × 17.37 × 4.56

III. RESULTS AND DISCUSSIONS

A. Structural properties of lipid bilayers upon dehydration

To investigate the effect of dehydration on the lateral organization of bilayers, the area per lipid (a_h) of the bilayers are calculated by

$$a_h = \left\langle \frac{b_x b_y}{N_l} \right\rangle, \tag{1}$$

where b_x and b_y are box lengths along x and y directions, respectively, N_l denotes the number of lipids in one leaflet, and angular brackets denote the time average. Figure S2 in the supplementary material shows the time evolution of area per lipid for different ω. Figure 2(a) shows that a_h of the bilayer falls off from ω = 10–4. Our results agree well with the area per lipid of different lipids obtained from different force-fields.[9,10] The lowering in a_h from ω = 10–4 indicates a chain ordering crossover in the bilayer at 308 K. The value of the area per lipid from ω = 45 to 4 is between fluid and gel phases (Table II), which might indicate the existence of the ordered phase at lower ω.

The thickness of bilayers (D_{HH}) is calculated using the following equation:

$$D_{HH} = \langle Z_l \rangle - \langle Z_u \rangle, \tag{2}$$

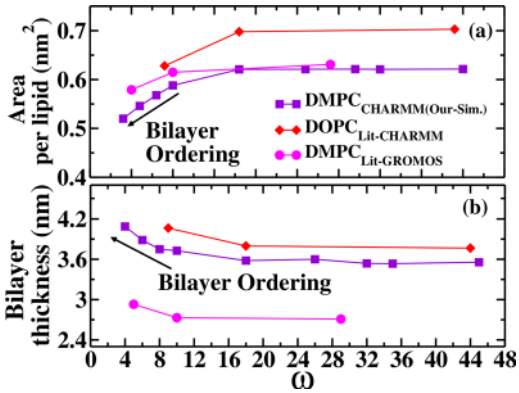

FIG. 2. (a) Area per lipid and (b) bilayer thickness with the change in hydration number for DMPC$_{CHARMM(our-sim.)}$, DOPC$_{Lit-CHAMRMM}$,[9] and DMPC$_{Lit-GROMOS}$.[10] The decrease in area per lipid and increase in bilayer thickness are found from ω = 10–4.

where $\langle Z_l \rangle$ and $\langle Z_u \rangle$ are time-averaged z-coordinates of the phosphorous heads obtained from the respective density profiles (Fig. S3 in the supplementary material). Similar to the a_h, the bilayer thickness remains constant above ω = 10 and then increases as the hydration number decreases [Fig. 2(b)]. Changes in both a_h and D_{HH} from ω = 10–4 indicate a crossover in bilayers due to dehydration. Our results show that ordering in the DMPC bilayer starts at ω = 10 at 308 K and the ordering increases until ω = 4. For DOPC lipids with CHARMM force-fields and DMPC lipids with GROMOS force-fields, a similar crossover happens at $\omega \sim 18$ and 10, respectively.[9,10] Our results are in good agreement with the experimental values[40,43] mentioned in Table II.

To investigate the alignment of chains with respect to the bilayer normal, the order parameter, $|S_{CD}|$,[10,55] has been calculated using following equation:

$$|S_{CD}| = \frac{1}{2}\langle 3\cos^2\theta - 1\rangle, \tag{3}$$

where θ is the angle between the bilayer normal and the C–H vector. Angular brackets denote an average over time and molecule. Figure 3(a) depicts the order parameter of DMPC chains with respect to the carbon number along the alkyl chains from ω = 45 to 4. Figure 3(b) shows the changes in order parameter averaged over the carbon numbers along the alkyl chain with ω. Distributions of angles between CH vectors and the bilayer normal are calculated for different CH along the chain and shown in Fig. S4 of the supplementary material. The distribution becomes narrower from ω = 45 to 4 with a shift in peaks for α CH and glyc. CH. A similar trend has been observed in previous simulations.[10] The distribution is moderately narrower from 45 to 4 without any shift in peak for tail 4 and 14 CH. Thus, the degree of ordering upon dehydration is more prominent in tail 4 and 14 CH than that in the α CH or glyc. CH. Importantly, the peaks of the angle distributions of the head to tail vector with the bilayer normal becomes significantly narrower from 45 to 4 near 15°, suggesting a crossover in chain ordering from high to low ω.

Table II represents the comparison of our results with existing literature from simulations and experiments for ω = 45 and 4. The values of a_h, D_{HH}, and $|S_{CD}|$ at ω = 45 from our calculations match well with the ones at a fluid phase obtained from simulation and experiments. Similarly, these values from our calculations at ω = 4 match well with the ones at a gel phase. Thus, by comparing the values of a_h, D_{HH}, and $|S_{CD}|$, bilayers at the full and least hydrations are identified as fluid and gel bilayers, respectively. Our analyses show that the bilayer has undergone a fluid-to-gel crossover when the water content is near ω = 10. This is consistent with previous molecular dynamics finding of bilayers undergoing a more ordered state upon lowering water contents.[10]

The thickness of the bilayer is calculated as a function of the bilayer surface, (x, y), as follows:

$$t(x,y) = \langle z_l(x,y) - z_u(x,y)\rangle. \tag{4}$$

where $z_l(x, y)$ and $z_u(x, y)$ are the z co-ordinates of the lipid head groups for the lower and the upper leaflets, respectively, as functions of the bilayer surface, (x, y). Angular brackets denote averaging over time. The thicknesses $t(x, y)$ are superimposed on the Voronoi area per lipid[56] for all hydration states using MATLAB.

TABLE II. Comparison of fully hydrated and dehydrated DMPC bilayers at 308 K from our simulations with fully hydrated fluid and gel phases at different temperatures from the literature.

			Literature	
Properties	ω	Our simulation (308 K)	Simulation	Experiment
Area per head group	45	0.62 ± 0.01	0.60 ± 0.02[41] (303 K), fluid	0.599 ± 0.12[40] (303 K), fluid
a_h (nm^2)	4	0.52 ± 0.03	0.50 ± 0.03[53] (273 K), gel	0.472 ± 0.05[54] (283 K), gel
Bilayer thickness	45	3.5	3.62[41] (303 K), fluid	3.6 ± 0.02[40] (303 K), fluid
D_{HH}(nm)	4	4.01	4.04 ± 0.05[53] (273 K), fluid	4.01 ± 0.01[54] (283 K), gel
Order parameter	45	0.19 ± 0.03	0.195 ± 0.03[38] (308 K), fluid	0.18[38] (303 K), fluid
$\|S_{CD}\|$	4	0.26 ± 0.02	0.25 ± 0.02[53] (273 K), gel	...

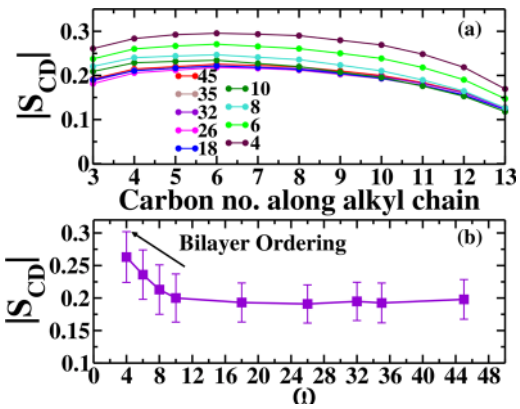

FIG. 3. (a) Order parameter with respect to the atom number along the alkyl chain and (b) averaged order parameter with respect to ω from 45 to 4. S_{CD} increases from ω = 10–4.

At ω = 45, the thickness of the bilayer is 3.6–4 nm, which varies a little (within 0.3–0.4 nm), indicating the fluid or liquid crystalline phase at the full hydration state [Fig. 4(a)]. Upon lowering ω, small domains of lower thicknesses arise in the bilayers that remain stable above ω = 10 [Figs. 4(b)–4(e)]. On lowering ω below 10, the variations in thickness on the bilayer surface disappear and the thicknesses increase, indicating chain ordering. Such homogeneous distributions of higher thickness of the bilayers remain stable until the lowest hydration number 4, demonstrating the existence of a gel phase at the lowest hydration. The thicknesses superimposed on the Voronoi area per lipid clearly show that for intermediate hydrated states, ω = 35–18, the bilayers have nano-sized regions or domains with lower and higher thicknesses.

To understand the structure of nano-domains better, interdigitation of chains are calculated as a function of surface (x, y) as follows:

$$I(x,y) = z_{l,end} - z_{u,end}, \tag{5}$$

where $z_{l,end}$ and $z_{u,end}$ are the z coordinates of the end beads of lower and upper leaflets, respectively. A comparison of the locations of the regions with lower thickness and interdigitation (Fig. S5 in the supplementary material) reveals that the nano-domains with lower thicknesses correspond to interdigitated chains (hydration number 45–18). The thickness increases in the gel phase, and the interdigitation disappears. This represents that bilayers have regions with the co-existence of ordered and disordered chains above ω = 10. From ω = 10, lipids start ordering by increasing the bilayer thickness and the bilayer undergoes a fluid-to-gel crossover near ω = 10.

B. Dynamical properties of IW

1. Survival probability of IW

Survival probabilities of water molecules near bilayers with different hydration numbers are computed using the following equation:

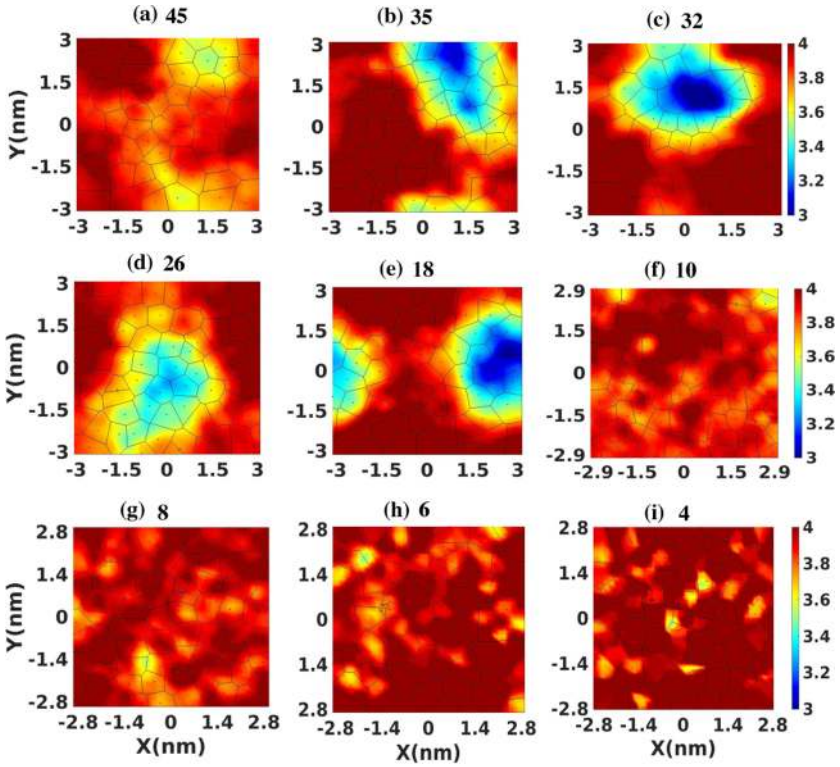

FIG. 4. Thickness superimposed on the Voronoi area per lipid head from the hydration number (a) 45 to (i) 4. The color bar is in nm. The bilayer undergoes a fluid-to-gel crossover upon lowering water contents.

$$S(t) = \sum_{i=1}^{N} \left\langle \prod_{t_k=t_0}^{t_0+t} P_i(t_k) \right\rangle, \tag{6}$$

where $S(t)$ is the probability of finding a water molecule residing in the interface layer at time t. N represents the total number of molecules, and angular bracket represents averaging over time origins t_0. $P_i(t) = 1$ if the molecule is present in the interface layer at time t and $P_i(t) = 0$ otherwise. Figure S6 in the supplementary material represents the survival probabilities of water near membranes at a fully hydrated state ($\omega = 45$) and at a dehydrated state ($\omega = 4$). The decay for $\omega = 4$ is slowest showing the highest survival probability of water upon dehydration. The residence time scales for the interface water are extracted by fitting the normalized survival probability to bi- or tri-exponential functions given by following equation:

$$y = A_f \exp(-t/\tau_f) + A_i \exp(-t/\tau_i) + A_s \exp(-t/\tau_s). \tag{7}$$

Interfacial water shows two or three characteristic time scales for $\omega = 45$ and 4, respectively. τ_f, τ_i, and τ_s represent fast, intermediate, and slow time scales. The extracted timescales (τ_f, τ_i, and τ_s) and the coefficients (A_s, A_i and A_f) from the fitting are presented in Table S1 in the supplementary material. Since the $S(t)$ of water decays completely, τ_s represents the residence time. From the fitting parameters shown in Table S1, it has been found that residence times (τ_s) of water near the bilayers with hydration numbers 45 and 4 are 123 and ~2621 ps, respectively. Since the water dynamics for $\omega = 45$ is fastest among all hydration numbers and 123 ps is the residence time of the interface water for the highest ω, the residence time of water for lower hydration numbers should be above 123 ps. Therefore, 100 ps is chosen as the confinement lifetime as this time scale is obeyed by interface water for all hydration numbers. Previously, 100 ps is found to be the residence time for IW.[57,58]

IW molecules are differentiated from remaining water molecules based on distance criteria.[57,59,60] Water molecules that reside *continuously* for 100 ps within ±0.35 nm of the peak location of phosphorous head group density of DMPC lipids are identified as IW. Figures 1(b) and 1(c) represent the snapshot of IW for hydration number 45 and 4, respectively.

2. Translational mean square displacement

To investigate the influence of dehydration on water dynamics and to find out its relation to a bilayer fluid-to-gel crossover, two dimensional (2D) translational mean square displacements (MSD_{XY}) of IW and lipid heads are calculated along the xy surface for different hydration numbers using the following equation:

$$\langle r^2(t) \rangle = \frac{1}{N} \sum_{i=1}^{N} \left\langle \left[r_i(t+t') - r_i(t') \right]^2 \right\rangle_{t'}, \tag{8}$$

where N represents the number of molecules, t' is the time origin, and t is the difference in time. The angular bracket represents average over time origins, t'. MSD_{XY} for the BW enters the diffusive regime (~t) within 0.3–0.4 ps [Fig. 5(a)]. As water contents are lowered, MSD_{XY} of the IW start decreasing and follow sub-diffusive behavior. A similar slowdown in water dynamics upon lowering water content has been observed in earlier experiments[18,20,59,61] and computational studies.[10,34,59,62] The slowdown in MSD_{XY} of the IW upon lowering ω is more prominent from $\omega = 10$–4. At $\omega = 4$, the MSD_{XY} of the IW develops a plateau. A similar trend in MSD_{XY} is followed by lipid heads at different ω, as shown in Fig. 5(b). The plateau in MSD_{XY} indicates an emergence of dynamical heterogeneity at low hydration.

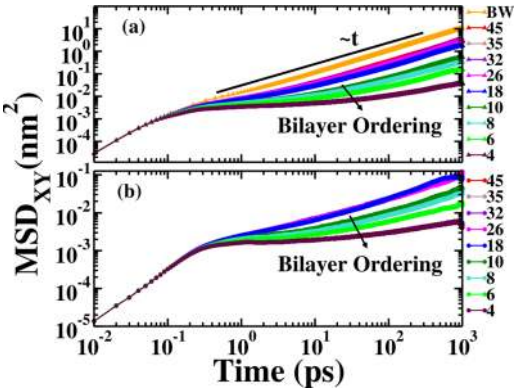

FIG. 5. Mean square displacements of (a) IW and (b) phosphorous heads of lipids along xy from hydration number 45–4. A prominent slowdown in MSD_{XY} has been observed for both IW and P from $\omega = 10$–4 once the bilayer starts ordering.

3. Non-Gaussian parameter

To check the existence of dynamical heterogeneity in IW due to dehydration, the 2D non-Gaussian parameter (NGP) is calculated by[63]

$$\alpha_2(t) = \frac{\langle \Delta r(t)^4 \rangle}{2\langle \Delta r(t)^2 \rangle^2} - 1. \tag{9}$$

$\alpha_2(t) = 0$, if NGP is truly a Gaussian, where $\Delta r(t) = r(t_0 + t) - r(t_0)$ is the particle displacement after a time interval t and the angular bracket represents ensemble averaging.

For the BW, NGP increases until ~1 ps and then starts decreasing, and by 20 ps, the NGP of the BW becomes zero, as shown in Fig. 6(a). This relaxation time for the BW is in good agreement with the previously reported time scale for the TIP4P/2005 water model[38] and neutron scattering experiments.[64] After 20 ps, the BW molecules show Gaussian dynamics and gradually enter in the diffusive region. For the IW molecules, the values of NGP are initially non-zero and slowly decrease to zero after 70 ns. Similar dynamical heterogeneity has been observed earlier for the IW hydrogen bonded to lipid head groups of a bilayer at room temperature.[57,65] The peak-heights of the NGPs increase once the water contents are lowered. The amplitude of the NGP increases significantly for the IW near the bilayer with ω from 10 to 4 in association with the bilayer ordering. The NGP of the IW near the bilayer with $\omega = 4$ has the highest peak manifesting the presence of significant amount of dynamical heterogeneity in the IW.

β to α relaxation time scales of the NGP are identified from the locations of their peaks and referred to as τ_{α_2}. As ω decreases, τ_{α_2}

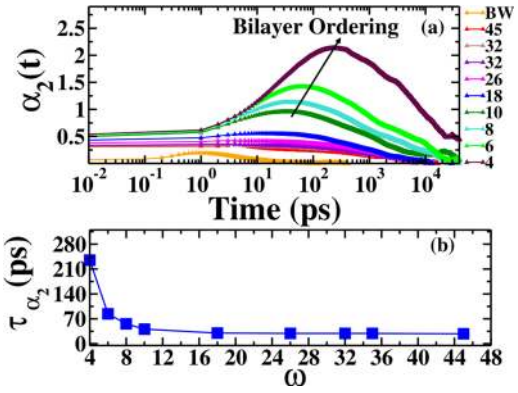

FIG. 6. (a) Non-Gaussian parameter [NGP, $\alpha_2(t)$] as a function of time and (b) changes in relaxation time scales (τ_{α_2}) with respect to the hydration numbers, ω. NGP shows a crossover at the onset of bilayer ordering.

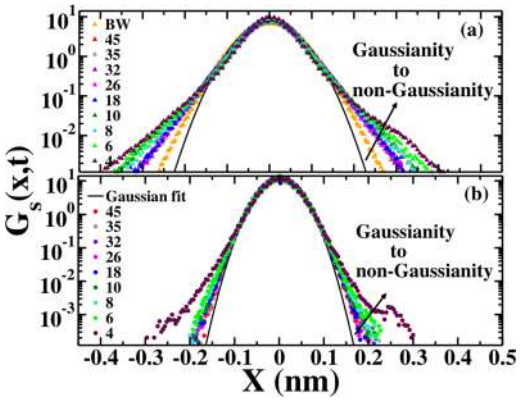

FIG. 7. Translational 1D van Hove correlation function of (a) IW and (b) phosphorous (P) heads from the hydration number 45–4. The distributions are more non-Gaussian in nature for both IW and P at $\omega = 4$.

increases, and for $\omega = 4$, there is a drastic increment in τ_{α_2} [Fig. 6(b)]. β to α relaxation time scales signify the correlation time scale of spatially heterogeneous dynamics and feature the crossover from cage to diffusive time scale for Brownian particles in a periodic effective field and polymer melts.[66,67] This clearly shows that at the dehydrated state, the IW molecules undergo a strong structural arrest and remain in the cage for much longer time compared to the ones at fully hydrated states. Thus, at lower hydration (from $\omega = 10$ until 4), the IW molecules exhibit glassy dynamics similar to supercooled liquids, while the BW molecules follow Fickian dynamics.[68]

4. van Hove correlation function

Since NGP of the IW shows characteristics of glassy dynamics, the self-part of the one dimensional (1D) van-Hove correlation function is calculated using the following equation:

$$G_s(\mathbf{r}, t) = \frac{1}{N}\left\langle \sum_{i=1}^{N} \delta(\mathbf{r} + \mathbf{r}_i(0) - \mathbf{r}_i(t)) \right\rangle. \tag{10}$$

$G_s(\mathbf{r}, t)$ are determined at time, and $t = 0.32$ ps for the BW. Figure 7(a) represents $G_s(\mathbf{r}, t)$ for the BW and the IW with various hydration numbers. The BW molecules follow a Gaussian distribution confirming the Fickian dynamics in the diffusive regime, which is in good agreement with the respective MSD_{XY}. $G_s(\mathbf{r}, t)$ for the IW are calculated at the time (shown in Table S2 in the supplementary material) when the IW show sub-diffusive behavior. $G_s(\mathbf{r}, t)$ for the IW becomes prominently non-Gaussian as the hydration numbers are lowered. A similar Gaussian to non-Gaussian transition in the van Hove correlation function has been observed for the lipid heads with lowering water contents in Fig. 7(b). The non-Gaussian nature of the van Hove correlation function is known to be the universal feature of dynamical heterogeneity in supercooled liquids.[69–74] The non-Gaussianity in the van Hove correlation function shows the underlying dynamics to be non-diffusive. Such non-diffusive dynamics has been observed earlier for water assisted conformational transitions of proteins.[75] This demonstrates that at lower hydration, both lipid and IW molecules start exhibiting dynamical heterogeneity with exponential tails in $G_s(\mathbf{r}, t)$, and such deviations from Gaussianity is most prominent for the lowest hydration state, $\omega = 4$. Thus, dehydration induces dynamical heterogeneity in the IW, which results in dynamical heterogeneity in the lipid bilayer facilitating the formation of gel bilayers seen in Fig. 4.

5. Self-intermediate scattering function

The self-intermediate scattering function (SISF) is another universal feature of dynamical heterogeneity. Since the bilayer is symmetric along the xy surface, the two dimensional SISF is calculated by following equation:

$$F_s(q, t) = \frac{1}{N}\left\langle \sum_{i=1}^{N} \cos(\mathbf{q}.[\mathbf{r}_i(t) - \mathbf{r}_i(0)]) \right\rangle, \tag{11}$$

where $q = \frac{2\pi}{\lambda}$ and λ is the wavelength. $\lambda = 0.50$ nm is chosen for the calculations of SISF as the first peak of $g(r)$ of IW, and phosphorous heads are at 0.3 nm and 0.6 nm, respectively (Fig. S7 in the supplementary material). Figure 8 shows the SISF of the BW and the IW near bilayers with $\omega = 45$–4. The BW decays to zero within 10 ps, whereas IW molecules for bilayers with different ω have much slower relaxations compared to the BW. Upon lowering water content, relaxation time scales of the SISF of the IW molecules increase. The relaxation is significantly slow once ω goes below 18. At $\omega = 4$, β and α relaxations are separated by a weak boson peak as seen for supercooled liquids.[76]

The α relaxation time scales (τ_α) are extracted for all cases when the SISF reaches the value of $1/e$, i.e., $F_s(q, t) = 1/e$. Since the SISF of the IW near the bilayer with $\omega = 4$ does not reach $1/e$ within 1 ns, the run-length of the bilayer is extended until 5 ns. Numerical values of the τ_α calculated for the IW molecules near the bilayers with different hydration numbers, ω, have been mentioned in Table III. The slowdown in α relaxation time with lowering water content shows that cage relaxations of IW molecules take longer time due to dehydration.

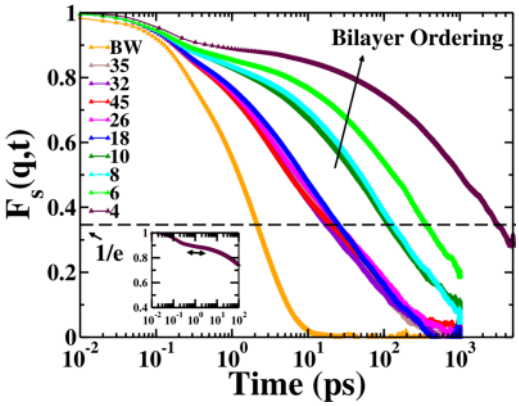

FIG. 8. SISF of IW for bilayers with ω = 45–4 at λ = 0.5 nm. Dashed line shows the value of $F_s(q, t)$ = 1/*e* to extract τ_α. The inset shows very weak boson peak for ω = 4.

To find out a relation between τ_α and the two dimensional diffusion co-efficient, D of IW, D has been obtained from the long time limit of MSD_{XY} by following the Einstein relation:

$$D = \lim_{t\to\infty} \langle r^2(t)\rangle/(4t). \tag{12}$$

The value of D of the BW from our simulation has been found to be 2.346 ± 0.026 × 10^{-5} cm^2 s^{-1}, which is in good agreement with previously performed simulation[38] and experiment.[77] The values of D of the IW at ω = 35 and 4 from our simulations using the TIP4P/2005 model are 1.46 ± 0.01 × 10^{-5} cm^2 s^{-1} and 0.0284 ± 0.0029 × 10^{-5} cm^2 s^{-1}, respectively. These values are slightly lower than the previously reported simulations[34] using the TIP3P water model as the TIP3P water model is known to have faster diffusion than the TIP4P/2005 water model.[38]

It is well known that a Brownian particle follows the Stokes–Einstein relation, $D \sim \tau_\alpha^{-1}$, at room temperature. The relation changes to the fractional Stokes–Einstein relation, $D \sim \tau_\alpha^{-\nu}$, where the scaling component $\nu < 1$ if the particles follow glassy behavior at lower temperature.[73,78–81] Experimental evidence of breakdown in the Einstein relation is found for supercooled confined water near a nano-pore or protein or methanol diluted bulk water using NMR and quasi-elastic neutron scattering spectroscopies.[82,83] In a binary harmonic sphere mixture of model glass-forming liquids, a breakdown of the Stokes–Einstein relation accompanied by a dynamic crossover in α-relaxation time with dynamic correlation length is found below and above the mode-coupling temperature.[84] Therefore, to investigate the changes in the IW dynamics due to dehydration, D is plotted with respect to τ_α. Figure 9 shows that the relation between D and τ_α of the IW follows Stokes–Einstein-like relation from ω = 45–18. The relation breaks to the fractional Stokes–Einstein-like relation where $\nu \sim 1$ changes to ν = 0.57 from ω = 10–4. A similar change in the scaling exponent has been observed when the pinning concentration is increased in randomly pinned glass-forming liquids at constant higher temperature,[85] demonstrating different dynamics at low and high pinning concentrations. As breakdown in the Stokes–Einstein relation indicate a crossover in dynamics[82,83] and an emergence in dynamical heterogeneity,[85] the change in the scaling exponent found in our work suggests that the IW molecules behave similar to glass-forming liquids once the water contents near the bilayer are from ω = 10–4. Interestingly, the change in ν in the IW is associated with the bilayer ordering (Fig. 4) for the same water content. This implies that dynamical heterogeneity in the IW due to the dehydration results in bilayer ordering.

TABLE III. The relaxation time scales obtained for different ω.

ω	τ_α (ps)	$\tau_{HB(RFA)}$ (ps)	$\tau_{HB(1/e)}$ (ps)
45	17.09	10.4	14.8701
35	18.23	13.8	16.89
32	15.11	3.9	10.79
26	21.09	9.71	15.95
18	102.64	9.71	15.95
10	115.23	21.27	15.99
8	115.23	32.25	78.04
6	322.13	142	300.14
4	3812	500	1426.11

6. Hydrogen bond auto-correlation functions

To understand the physical origin of dynamical heterogeneity due to dehydration, hydrogen bond auto-correlation functions [HBACF, $C_{HB}(t)$] are calculated using the following equation:[86–88]

$$C_{HB}(t) = \frac{\langle h_{IW}(0)h_{IW}(t)\rangle}{\langle h_{IW}\rangle}, \tag{13}$$

where $h_{IW}(t)$ denotes hydrogen bonds among the BW or the IW. $h_{IW}(t)$ will be 1 if there is a hydrogen bonding; else, it will be 0. The hydrogen bonds are allowed to break and reform, and thus, $C_{HB}(t)$ represents the intermittent hydrogen bond auto-correlation

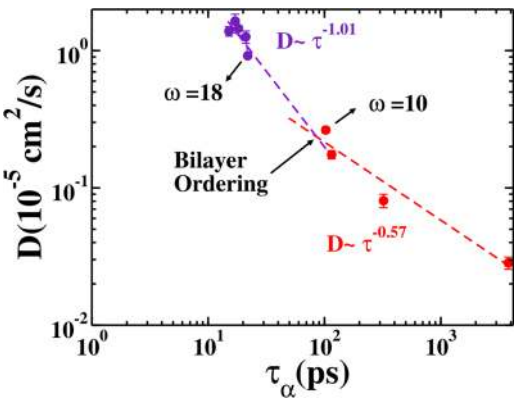

FIG. 9. Diffusion constant, D, vs τ_α showing a dynamical crossover near ω = 10. The crossover is associated with bilayer ordering.

function. The probability of a specific hydrogen bond remains intact and is zero at equilibrium in a large system. Thus, $C_{HB}(t)$ relaxes to zero at equilibrium. The HBACF of the BW decays fastest compared to that of the IW, as seen from Fig. 10, similar to the previous observations.[33,86,89] HBACFs of the IW molecules remain correlated significantly for a longer time from ω = 10–4 when the bilayer starts ordering. The HBACFs of the IW are slowest for the lowest $\omega = 4$, suggesting that the hydrogen bond dynamics is most hindered for the IW molecules with the lowest ω. Reactive flux analysis has been used to understand the kinetics of hydrogen bond formation or breaking.[88,90,91] The rate of relaxation $[K(t)]$ of $C_{HB}(t)$ to equilibrium is calculated by

$$K(t) = -\frac{dC_{HB}(t)}{dt}. \tag{14}$$

where $K(t)$ can be expressed in terms of the forward rate constant (k) and the backward rate constant (k') as follows:

$$K(t) = kC_{HB}(t) - k'n(t). \tag{15}$$

Here, $n(t)$ represents the population of broken hydrogen bonds that was present at $t = 0$. Note these hydrogen bond partners may still reside within the hydrogen bond distance. The kinetic parameters, k and k', are shown with respect to ω in Fig. S8(a) of the supplementary material. Both the hydrogen bond breaking (forward) and formation (backward) rate constants of the interface water show a crossover near ω = 10. Since the number of interface water molecules increase upon lowering the hydration number (Table S3 in the supplementary material), the numbers of average hydrogen bonds follow a similar trend [Fig. S8(b) in the supplementary material]. Using the forward rate constant (k), the lifetime of hydrogen bonding is calculated by

$$\tau_{HB(RFA)} = \frac{1}{k}. \tag{16}$$

Numerical values of the $\tau_{HB(RFA)}$ calculated using reactive flux analysis (RFA) for the IW molecules near the bilayers with different hydration numbers have been mentioned in Table III. Since the forward rate constants decrease with lowering hydration numbers, $\tau_{HB(RFA)}$ increases upon dehydration. The values of $\tau_{HB(RFA)}$ are compared with the hydrogen bond lifetimes ($\tau_{HB(1/e)}$) obtained from $1/e$ values of $C_{HB}(t)$.

7. Behavior of relaxation times with hydration numbers

To investigate the behavior of different relaxation times of the IW due to the change in the hydration numbers, the α relaxation times (τ_α) extracted from $F_s(q, t)$ are compared with the hydrogen bond lifetimes calculated using both methods of reactive flux analysis (RFA) and $1/e$. These time scales have been plotted with respect to ω in Fig. 11. The nature of $\tau_{HB(RFA)}$ and $\tau_{HB(1/e)}$ with respect to ω shows the comparison of ω dependence of hydrogen bond lifetimes from both methods. The growing relaxation time scales of $\tau_{HB(RFA)}$ and $\tau_{HB(1/e)}$ toward the lower hydration shows that the hydrogen bonds of the IW remain intact for a significantly longer period of time from ω = 10–4. A similar longer hydrogen bond lifetime for the dehydrated state of the DMPC bilayer was reported earlier.[34] Interestingly, the relaxation time scales of τ_α and τ_{HB} follow similar crossovers near ω = 10. This indicates that the nature of the α relaxation times of IW can be reflected in the hydrogen bond lifetimes. This suggests that the hydrogen bond dynamics are the physical origin of long time relaxations obtained from the $F_s(q, t)$. In a previous work, chemically confined IW molecules near a fluid bilayer are found to exhibit similar characteristics.[65]

The relaxation times vs different hydration numbers in Fig. 11 can be fitted by the Vogel–Fulcher–Tamman (VFT)[85,92,93] like equation given as follows:

$$\tau = \tau_0 \exp\left(\frac{K\omega_0}{\omega - \omega_0}\right). \tag{17}$$

Here, ω_0 quantifies the hydration number characterizing a fluid-to-gel crossover in the bilayer, and K is the fragility parameter. The fitting parameters in Table IV show that the characteristic hydration

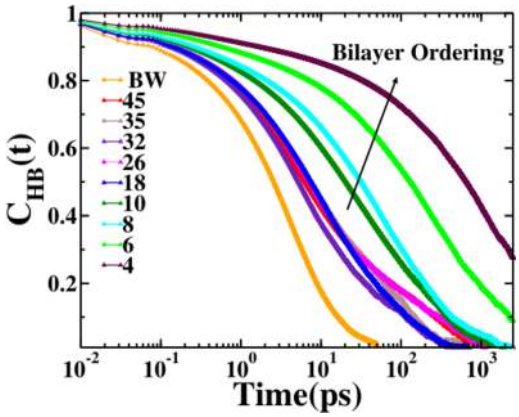

FIG. 10. Hydrogen bond auto-correlation function of BW and IW near bilayers with different ω from 45 to 4.

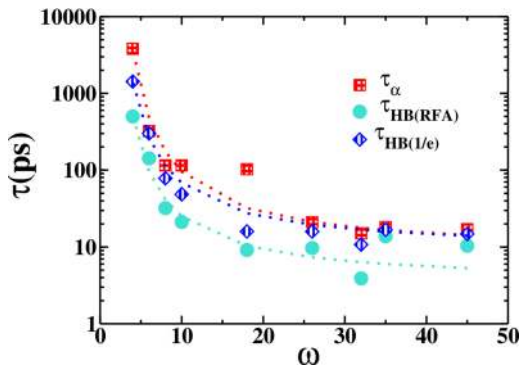

FIG. 11. Changes in relaxation time scales, τ, with respect to the hydration numbers, ω. τ_α obtained from $F_s(q, t)$ and τ_{HB} obtained from both reactive flux analysis (RFA) and 1/e value of $C_{HB}(t)$ follow similar crossovers from ω = 10–4.

TABLE IV. VFT fitting parameters.

τ	τ_0 (ps)	K	ω_0
τ_α	327 460	2.3	10.47
$\tau_{HB(1/e)}$	198 728	2.03	10.02
$\tau_{HB(RFA)}$	80 000	2.01	10.1

number is $\omega \sim 10$ at which the bilayer transforms from a fluid/ripple-like phase to a gel-like phase. This result is in agreement with Fig. 9 and with all our calculations, which indirectly show that the bilayer starts ordering from $\omega \sim 10$. Below 10, the bilayer remains in an ordered or gel-like state. At the onset of the bilayer ordering, there is an emergence of dynamical heterogeneity in the IW molecules near the bilayer.

8. Reorientational auto-correlation function (RACF)

To understand the influence of hydration numbers on the rotational dynamics of water, the reorientational auto-correlation function (RACF) is calculated for the IW for different hydration numbers and the BW. The RACF, $C_{vl}(t)$, of water is calculated by the following equation:

$$C_{vl}(t) = \frac{\langle \sum_{i=1}^{N} P_l[e_i^v(t) \cdot e_i^v(0)] \rangle}{\langle \sum_{i=1}^{N} P_l[e_i^v(0) \cdot e_i^v(0)] \rangle}, \tag{18}$$

where $e_i^v(t)$ represents the vector for which the RACF is calculated and P_l is the lth order Legendre polynomial. $C_{vl}(t)$ are computed for the first ($l = 1$) and the second order ($l = 2$) Legendre polynomial for the OH bond vector ($\vec{OH}$), the HH bond vector ($\vec{HH}$), and the dipole moment vector $\vec{\mu}$. Figures 12(a) and 12(b) shows that the RACF for the first and second order Legendre polynomials, respectively, for the IW and the BW.

The RACFs of the BW much rapidly decay to zero compared to that of the IW showing a faster relaxation to the equilibrium. The $C_{v2}(t)$ decreases faster than the $C_{v1}(t)$ for all cases. Both $C_{v1}(t)$ and $C_{v2}(t)$ for all cases exhibit slower decay as the hydration number decreases. The RACF for the IW water for the ω = 45–18 overlap with each other shows no difference in orientations. The RACF of the IW significantly differ from ω = 10 onward at the onset of the bilayer ordering. The most preferred orientations of the IW are obtained at ω = 4 for all cases. A similar slowdown in the rotational relaxation has been observed in water near DMPC and DLPC bilayers.[34,62] The preferred orientations of the IW for the lower ω are attributed to the persistent hydrogen bonds with longer lifetime. Earlier calculations suggest that the probability of hydrogen bonds between IW and lipids increases as the hydration number decreases and most of the water reside in the interior of the membrane.[34] Upon dehydration, bound water bridging lipids increases with longer lifetime of lipid–water hydrogen bonds. At the same time, the fraction of the lipid unbound water decreases. Since the structure of bound and unbound water to the lipids are different due to the hydrogen bond network and coordination defects,[100,101] the residence time of bound water increases changing the lipid mobility and membrane fluctuations. The significant slowdown in the RACF of the IW in association with the bilayer ordering indicates a coupling between the rotational dynamics of the IW with the bilayer phase change.

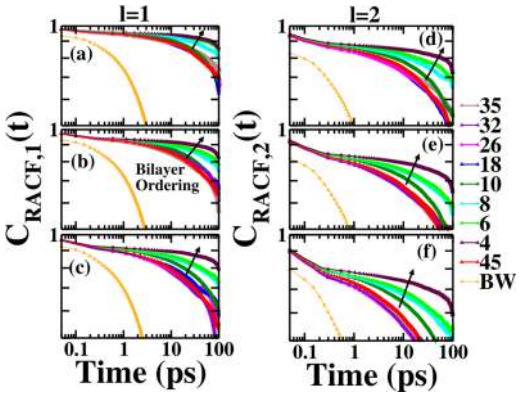

FIG. 12. RACF of the IW and bulk water for $\vec{OH}$ [(a) and (d)], $\vec{HH}$ [(b) and (e)], and $\vec{\mu}$ [(c) and (f)] for l = 1 and 2.

9. Dynamics of the lateral organization of the bilayer

The two dimensional (2D) van Hove correlation function of the lipid phosphorous head is calculated by the following equation:[94]

$$G_s^{simulation}(\mathbf{r}, t) = \frac{1}{N}\left\langle \sum_{i=1}^{N} \delta(\mathbf{r} + \mathbf{r}_i(0) - \mathbf{r}_i(t)) \right\rangle. \tag{19}$$

Here, r is the displacement of the phosphorous head of the lipid at time t. The calculation is done for a 40 ns run-length. It is well known that the van Hove correlation function of the Brownian particles should obey a Gaussian distribution. Thus, to measure the deviations of the 2D van Hove of lipids from that of the Brownian particles, the theoretical van Hove correlation function G^{theory} is calculated in two dimensions by the following equation:[95]

$$2\pi r G^{theory}(r, t) = \frac{2r}{\langle r^2(t) \rangle} \exp^{\frac{-r^2}{\langle r^2(t) \rangle}}. \tag{20}$$

Here, $\langle r^2(t) \rangle$ is the two dimensional mean square displacement along x and y at time t. $G_s^{simulation}(r, t)$ and $G_s^{theory}(r, t)$ cross each other at two characteristics distances r_1 and r_2. These two distances are considered as the cutoffs for the particles that remain within the cage and that undergo jump.[95] If the displacement of a particle $r < r_1$, the particle is tagged as a particle within a cage. If the displacement of a particle $r > r_2$, the particle is tagged as a mobile particle. Figure 13 shows the simulated and theoretical 2D van Hove correlation functions for the phosphorous heads for different ω. The $G_s^{simulation}(r, t)$ do not deviate much from the $G_s^{theory}(r, t)$ above ω = 10, confirming the fluid phase of the bilayer, as seen in Fig. 4. At the onset of the bilayer ordering near ω = 10, the differences between $G_s^{simulation}(r, t)$ and $G_s^{theory}(r, t)$ are much prominent. At

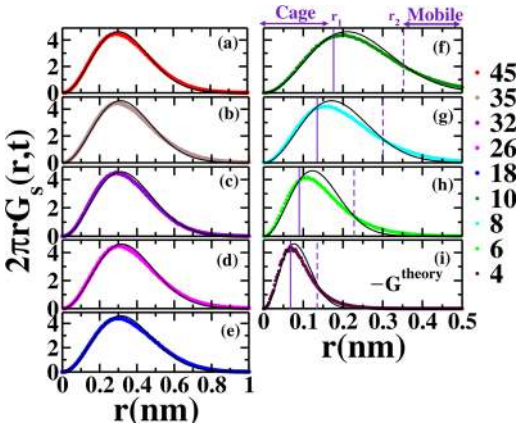

FIG. 13. 2D van Hove correlation functions for P (a) 45 to (i) 4; dotted lines—$G_s^{simulation}$ and solid black lines—G_s^{theory}. Maximum deviation from the Gaussianity has been found at $\omega = 4$. The deviation clearly demonstrates non-Brownian motions in lipid heads due to heterogeneity of lipids in the gel phase.

$\omega = 4$, the deviations are significant, demonstrating the gel phase of the bilayer. Both the cutoff distances, r_1 and r_2, reduce upon lowering ω (Fig. 14). The cutoff r_1 ranges between 0.4 and 0.15 nm so that the mean square displacements of mobile lipid heads $[\langle r^2_{mobile}(t)\rangle^{1/2} = 2r_2]$ vary from 0.8 nm to 0.3 nm. The displacements are slightly larger than the inter-molecular spacing ~0.6 to 0.3 nm obtained from the location of the first peak of $g(r)$ (Fig. S7 in the supplementary material) or the σ value of the non-bonded Lennard-Jones potential. Thus, at the onset of bilayer ordering near $\omega = 10$, two distinct classes of mobility groups are found for the bilayer: few lipids remain within the cage cutoff distance r_1, and few lipids escape these cages and move beyond the distance of intermolecular spacing, suggesting a "molecular replacement mechanism" in lipid dynamics. This feature has been observed earlier for coarse-grained DPPC

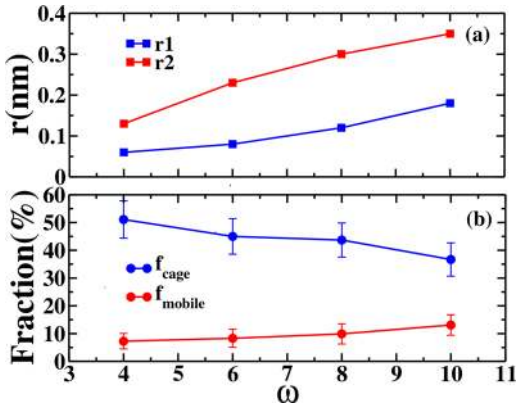

FIG. 14. (a) Cutoff displacements, r_1 and r_2, vs different hydration numbers, ω, where r_1 and r_2 represent displacements for the cage and mobile particles, respectively. (b) Fractions of lipids with cage and mobile particles with respect to ω.

TABLE V. Fractions of caged (f_{cage}) and mobile (f_{mobile}) lipids with different hydration numbers.

ω	f_{cage} (in %)	f_{mobile} (in %)
10	36.7	13.1
8	43.7	9.9
6	45.0	8.3
4	51.1	7.26

lipids in the gel phase.[94] The fractions of caged and mobile lipids ($f_{cage/mobile}$) are calculated after averaging over 39 000 frames for 40 ns run-lengths using the following equation:

$$f_{cage/mobile} = \frac{\langle n_{cage/mobile}\rangle}{N}, \tag{21}$$

where $\langle n\rangle$ is the time averaged number of caged or mobile lipids based on the cutoff distances, r_1 and r_2, respectively, and N is the total number of lipids. Table V represents the fractions of the caged and mobile lipids in bilayers with different hydration numbers. The fraction of caged lipids increase and the mobile lipids decrease upon lowering hydration numbers below 18. At $\omega = 4$, the fraction of the mobile lipids is minimum, and the fraction of the caged lipids is more than 50%, resulting in an ordered bilayer or a gel phase. Note that for all these cases, there can be another kind of lipids that are neither confined within a cage nor completely mobile after cage relaxations. These distinct mobility groups are not visible for the fluid phase above $\omega = 10$.

To visualize the lateral organizations of the bilayers at high and low hydration numbers, phosphorous heads are color coded as caged and mobile particles based on the cutoff distances for a single snapshot. If the displacement of a lipid head remains within the cage at any instant of time, the head is tagged with green color. Similarly, if the displacement of a lipid head is greater than r_2, the lipid head is considered as a mobile particle and shown in blue. Figure 15(a) shows that all particles are mobile (blue) in the fluid phase as there are no distinct mobility groups present. In the gel phase at hydration number $\omega = 4$, the bilayer [Fig. 15(b)] has two

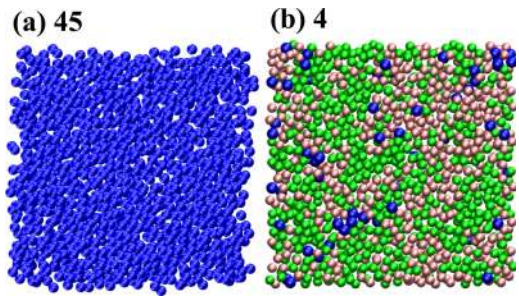

FIG. 15. Snapshots of mobile and caged atoms in VDW (van der Waals) representations at (a) 45 and (b) 4. Blue: mobile; green: caged.

classes of lipids with ~50% caged particles with strong structural arrest in combination with very few mobile particles. The number of clusters and maximum size of the clusters for caged and mobile lipid heads at different hydrations are calculated. Upon dehydration, the maximum size of the clusters increases for caged lipids and decreases for mobile lipids with an opposing effect on the number of clusters [Figs. S9(a), S9(b), S9(d), and S9(e) in the supplementary material]. This indicates the growth of the cluster size of caged lipids at the cost of reduction of clusters of mobile lipids on lowering the hydration numbers. Unlike the reported mobile lipids in the coarse-grained DPPC lipid gel phase at 300 K,[94] the mobile particles do not form any cluster in the present dehydration induced gel phase and are dispersed throughout the bilayer surface, indicating no spatial correlation within the mobile lipids. However, the caged lipids stick together forming clusters or continuous nanodomains spanning across the bilayer surface [Fig. 15(b)]. It is known that the fractal dimension of the largest cluster characterizes the location of a true percolation threshold.[96–99] Percolation transition happens if the fractal dimension reaches a value of 91/48 in two dimensions since any object only with fractal dimension greater than 91/48 can be infinite. The fractal dimension of the largest cluster can be calculated from the fitting of the cumulative radial distribution function [$m(r)$] as

$$m(r) \sim r^{d_f}, \tag{22}$$

where d_f is the dimension of the fractal. Figures S9(c) and S9(f) of the supplementary material shows that $m(r)$ of caged and mobile lipids do not follow a scaling relation as in Eq. (22). The fitted lines to Eq. (22) are shown in solid black lines in Figs. S9(c) and S9(f) of the supplementary material. The deviations of the fitted data after 0.5 nm indicate that the clusters of caged lipids may not obey percolation. Similar results have been obtained in three dimensions (data not shown).

IV. CONCLUSION

We have investigated the structural and dynamical properties of DMPC lipid bilayers by lowering hydration numbers at 308 K using all-atom MD simulations. The decrease in the area per head group and increase in the bilayer thickness superimposed on the bilayer surface and order parameter of lipids upon dehydration clearly demonstrate that the bilayer undergoes moderate structural ordering with a fluid-to-gel crossover when the hydration number (ω) reduces to 10. The structural properties of the bilayers obtained from our simulations are in good agreement with experimental and simulated values in the literature.[9,10,38,40,41,53] In order to understand the role of water in such structural changes of the bilayer, interface water (IW) molecules are identified based on geometric criteria and their residence times. The MSD_{XY} of both the IW and lipid heads show more sub-diffusive behavior on lowering the water contents. The plateau in the MSD_{XY} of the IW at the dehydrated state indicates a possibility of glass-like behavior of the IW at room temperature.

To confirm the presence of glassy behavior of the IW, the non-Gaussian parameters of the IW are calculated for all ω. The β to α relaxation times slow down from the hydration number 10–4, manifesting the emergence of dynamical heterogeneity in the IW at the onset of bilayer ordering upon dehydration. This is attributed to a strong structural arrest of the IW in a cage for longer time at lower water contents. 1D van Hove correlation functions of both the IW and phosphorous head atoms exhibit significant non-Gaussianity, manifesting non-diffusive behavior of both the IW and the lipid heads at lower water contents. To obtain the structural relaxation of the IW, SISF is calculated for the IW near the bilayers with different hydration numbers. Relaxations of the SISF of the IW slow down on approaching lower water contents. At the dehydrated state ($\omega = 4$), a very weak boson peak indicated by a small region of plateau separating the β and α relaxations in the SISF of the IW has emerged. A similar boson peak arises for glass-forming liquids with lowering in temperature.[76] Such a plateau-like region in the SISF of the IW with respect to time provides a measure of the extent of structural arrest in the IW due to dehydration. The structural relaxation times obtained from the SISF of the IW slow down upon lowering in water contents. The structural relaxation time and the diffusion constant obtained from the linear region of the MSD_{XY} obey the Stokes–Einstein relation as $D \sim \tau_\alpha^{-1}$ at room temperature for the IW above $\omega = 10$. On the onset of the bilayer ordering near $\omega = 10$, a dynamical crossover in the τ_α has been observed where $D \sim \tau_\alpha^{-0.57}$. This observation is reminiscent of the fractional Stokes–Einstein relation found for confined supercooled water using experiments or for a binary mixture of model glass-forming liquids.[82–84] This clearly shows that the dehydration in the bilayer induces an emergence of dynamical heterogeneity in the IW in association with bilayer ordering. To find out the physical origin of the dynamical heterogeneity in the IW, HBACFs are calculated for the IW at different hydration states. The decay in HBACF slows down significantly from $\omega = 10$–4 when the bilayer starts ordering. Using reactive flux analysis, the hydrogen bond lifetime τ_{HB} has been calculated for the IW at different ω. Interestingly, the α relaxation time, τ_α, follows similar behavior as the τ_{HB} with a rise near $\omega = 10$, suggesting that the hydrogen bonds are the physical origin of the τ_α of the IW. The behavior of both the relaxation times (τ_{HB} and τ_α) with ω are fitted to the VFT-like equation to obtain a characteristic hydration number $\omega = 10$ indicating a crossover. Note our previous analysis shows that the bilayer undergoes the fluid-to-gel crossover at the same ω. The rotational auto-correlation function (RACF) of the IW is calculated for both the first and second order Legendre polynomials. The rotational relaxations of the IW fall off at significantly longer times once the hydration numbers are from 10 to 4. A significant slowdown in the rotational relaxation in association with the bilayer ordering indicates a coupling between rotational dynamics of the IW with the bilayer ordering. The preferred orientation of the IW due to longer hydrogen bond lifetime facilitates shrinkage in the area per head group at lower hydration and increase in bilayer ordering. Although dynamics of the interface water and local lipids are affected strongly due to dehydration in association with bilayer ordering, the structural changes in bilayers are comparatively moderate in nature. This is consistent with previous molecular dynamics findings.[10]

To understand the effect of dynamical heterogeneity on the lipid displacements during the fluid-to-gel crossover, 2D van Hove correlation functions of the lipid phosphorous head groups are calculated at different ω. Above $\omega = 10$, the simulated van Hove correlation functions of lipid heads match well with the theoretical

van Hove correlation functions for the Brownian particles. The Brownian nature of the displacements of the lipid heads confirms the fluidic, L_α phase of the bilayer above $\omega = 10$. Below this, the simulated van Hove correlation functions of lipid heads deviate from the theoretical ones with two characteristic cutoff distances r_1 and r_2, both of which decay upon lowering ω. These two cutoffs r_1 and r_2 provide spatial measures of cage and mobile particles, respectively. At the onset of the bilayer ordering, the fraction of the caged lipid molecules increases with lowering in water content with a decrease in the fraction of the mobile lipid molecules. The mobile lipids move slightly larger than the intermolecular spacing of the lipids, suggesting a possibility of the existence of the molecular displacement mechanism observed earlier for the gel phase of the coarse-grained DPPC bilayer.[94] This clearly demonstrates that the spatial distribution of lipid dynamics becomes heterogeneous in nature upon dehydration. In contrast to the previous observation for the gel phase of the coarse-grained DPPC bilayer, no cluster is formed by the mobile particles in the gel phase obtained by the dehydration. Instead, the cluster of caged lipids spans all over the bilayer surface. Preliminary results suggest no percolation in the clusters of caged lipids. Such a difference in the spatial distribution of lipid dynamics reveals that the spatiotemporal correlations in the gel phase obtained by the dehydration can be different than those obtained by cooling. The dehydration induces non-Brownian dynamics to the lipids originating from distinct mobility groups, which results in the formation of the gel phase. Thus, the present analysis unfolds the mechanism of fluid-to-gel crossover of the bilayer assisted by growing relaxation time scales of the interface water and dynamical heterogeneity due to the dehydration. This clearly suggests that the structural changes of the bilayers are correlated with the dynamics of the interface water upon dehydration. A similar phenomenon has been observed earlier for surfactant membranes due to lowering in temperature using molecular dynamics simulations.[60] Thus, the present work enhances our fundamental understanding on the membrane dehydration and can help in mimicking cryogenic behavior of membranes at room temperature. Our analyses pave the way of finding controlling parameters to achieve functionally relevant nano-domain formations in complex bio-membranes under anhydrobiosis conditions.

SUPPLEMENTARY MATERIAL

See the supplementary material for the plots of mean square displacements of phosphorous heads, the time evolutions of the area per head group of lipids, density profiles of lipid heads, thickness and interdigitation of bilayers superimposed on the Voronoi area per lipid head, kinetic parameters for hydrogen bond breaking and formation and number of average hydrogen bonds for all ω, distributions of angles between CH vectors and the bilayer normal, survival probabilities of IW, radial distribution functions of P heads and IW, number of clusters, maximum size of clusters, and cumulative radial distribution functions of caged and mobile particles for different ω. Tables for fitted parameters of survival probabilities for $\omega = 45$ and 4, number of IW molecules, and time scales at which van Hove correlation functions of IW are calculated are also shown for $\omega = 45$–4.

ACKNOWLEDGMENTS

We acknowledge the financial support of Grant No. SERB CRG/2019/000106. A.D. is thankful to Prabhat Jaiswal for useful discussions.

DATA AVAILABILITY

The data that support the findings of this study are available from the corresponding author upon reasonable request.

REFERENCES

[1] J. Milhaud, "New insights into water–phospholipid model membrane interactions," Biochim. Biophys. Acta **1663**, 19–51 (2004).
[2] S. Tan, T. Wu, D. Zhang, and Z. Zhang, "Cell or cell membrane-based drug delivery systems," Theranostics **5**, 863 (2015).
[3] I. W. Hamley, *Introduction to Soft Matter: Synthetic and Biological Self-Assembling Materials* (John Wiley & Sons, 2013).
[4] J. H. Crowe, F. A. Hoekstra, and L. M. Crowe, "Anhydrobiosis," Annu. Rev. Physiol. **54**, 579–599 (1992).
[5] A. Trounson and L. Mohr, "Human pregnancy following cryopreservation, thawing and transfer of an eight-cell embryo," Nature **305**, 707–709 (1983).
[6] J. H. Crowe and L. M. Crowe, "Preservation of mammalian cells—Learning nature's tricks," Nat. Biotechnol. **18**, 145–146 (2000).
[7] K. L. Koster, M. S. Webb, G. Bryant, and D. V. Lynch, "Interactions between soluble sugars and POPC (1-palmitoyl-2-oleoylphosphatidylcholine) during dehydration: Vitrification of sugars alters the phase behavior of the phospholipid," Biochim. Biophys. Acta **1193**, 143–150 (1994).
[8] K. Gawrisch, D. Ruston, J. Zimmerberg, V. A. Parsegian, R. P. Rand, and N. Fuller, "Membrane dipole potentials, hydration forces, and the ordering of water at membrane surfaces," Biophys. J. **61**, 1213–1223 (1992).
[9] S. S. Stachura, C. J. Malajczuk, E. Kuprusevicius, and R. L. Mancera, "Influence of bilayer size and number in multi-bilayer DOPC simulations at full and low hydration," Langmuir **35**, 2399–2411 (2019).
[10] C.-J. Högberg and A. P. Lyubartsev, "A molecular dynamics investigation of the influence of hydration and temperature on structural and dynamical properties of a dimyristoylphosphatidylcholine bilayer," J. Phys. Chem. B **110**, 14326–14336 (2006).
[11] E. Persson and B. Halle, "Cell water dynamics on multiple time scales," Proc. Natl. Acad. Sci. U. S. A. **105**, 6266–6271 (2008).
[12] P. Jungwirth, "Biological water or rather water in biology?," J. Phys. Chem. Lett. **6**, 2449–2451 (2015).
[13] M. R. Brzustowicz and A. T. Brunger, "X-ray scattering from unilamellar lipid vesicles," J. Appl. Crystallogr. **38**, 126–131 (2005).
[14] A. H. de Vries, I. Chandrasekhar, W. F. van Gunsteren, and P. H. Hünenberger, "Molecular dynamics simulations of phospholipid bilayers: Influence of artificial periodicity, system size, and simulation time," J. Phys. Chem. B **109**, 11643–11652 (2005).
[15] X. Lin, V. Nair, Y. Zhou, and A. A. Gorfe, "Membrane potential and dynamics in a ternary lipid mixture: Insights from molecular dynamics simulations," Phys. Chem. Chem. Phys. **20**, 15841–15851 (2018).
[16] S. K. Pal, J. Peon, B. Bagchi, and A. H. Zewail, "Biological water: Femtosecond dynamics of macromolecular hydration," J. Phys. Chem. B **106**, 12376–12395 (2002).
[17] K. Murzyn, W. Zhao, M. Karttunen, M. Kurdziel, and T. Róg, "Dynamics of water at membrane surfaces: Effect of headgroup structure," Biointerphases **1**, 98–105 (2006).
[18] S. R. Wassall, "Pulsed field gradient-spin echo NMR studies of water diffusion in a phospholipid model membrane," Biophys. J. **71**, 2724–2732 (1996).
[19] S. König, E. Sackmann, D. Richter, R. Zorn, C. Carlile, and T. M. Bayerl, "Molecular dynamics of water in oriented DPPC multilayers studied by quasielastic

neutron scattering and deuterium-nuclear magnetic resonance relaxation," J. Chem. Phys. **100**, 3307–3316 (1994).
[20]W. Zhao, D. E. Moilanen, E. E. Fenn, and M. D. Fayer, "Water at the surfaces of aligned phospholipid multibilayer model membranes probed with ultrafast vibrational spectroscopy," J. Am. Chem. Soc. **130**, 13927–13937 (2008).
[21]K. J. Tielrooij, D. Paparo, L. Piatkowski, H. J. Bakker, and M. Bonn, "Dielectric relaxation dynamics of water in model membranes probed by terahertz spectroscopy," Biophys. J. **97**, 2484–2492 (2009).
[22]M. Trapp, T. Gutberlet, F. Juranyi, T. Unruh, B. Demé, M. Tehei, and J. Peters, "Hydration dependent studies of highly aligned multilayer lipid membranes by neutron scattering," J. Chem. Phys. **133**, 10B615 (2010).
[23]X. Chen, W. Hua, Z. Huang, and H. C. Allen, "Interfacial water structure associated with phospholipid membranes studied by phase-sensitive vibrational sum frequency generation spectroscopy," J. Am. Chem. Soc. **132**, 11336–11342 (2010).
[24]J. A. Mondal, S. Nihonyanagi, S. Yamaguchi, and T. Tahara, "Three distinct water structures at a zwitterionic lipid/water interface revealed by heterodyne-detected vibrational sum frequency generation," J. Am. Chem. Soc. **134**, 7842–7850 (2012).
[25]E. Yamamoto, T. Akimoto, M. Yasui, and K. Yasuoka, "Origin of subdiffusion of water molecules on cell membrane surfaces," Sci. Rep. **4**, 4720 (2014).
[26]C. Ho, S. J. Slater, and C. D. Stubbs, "Hydration and order in lipid bilayers," Biochemistry **34**, 6188–6195 (1995).
[27]G. Cevc and D. Marsh, "Hydration of noncharged lipid bilayer membranes. Theory and experiments with phosphatidylethanolamines," Biophys. J. **47**, 21–31 (1985).
[28]T. Fukuma, M. J. Higgins, and S. P. Jarvis, "Direct imaging of individual intrinsic hydration layers on lipid bilayers at ångstrom resolution," Biophys. J. **92**, 3603–3609 (2007).
[29]M. J. Higgins, M. Polcik, T. Fukuma, J. E. Sader, Y. Nakayama, and S. P. Jarvis, "Structured water layers adjacent to biological membranes," Biophys. J. **91**, 2532–2542 (2006).
[30]L. Tayebi, Y. Ma, D. Vashaee, G. Chen, S. K. Sinha, and A. N. Parikh, "Long-range interlayer alignment of intralayer domains in stacked lipid bilayers," Nat. Mater. **11**, 1074–1080 (2012).
[31]H. Binder, "Water near lipid membranes as seen by infrared spectroscopy," Eur. Biophys. J. **36**, 265–279 (2007).
[32]M. Doxastakis, V. Garcia Sakai, S. Ohtake, J. K. Maranas, and J. J. De Pablo, "A molecular view of melting in anhydrous phospholipidic membranes," Biophys. J. **92**, 147–161 (2007).
[33]C. Calero and G. Franzese, "Membranes with different hydration levels: The interface between bound and unbound hydration water," J. Mol. Liq. **273**, 488–496 (2019).
[34]C. Calero, H. E. Stanley, and G. Franzese, "Structural interpretation of the large slowdown of water dynamics at stacked phospholipid membranes for decreasing hydration level: All-atom molecular dynamics," Materials **9**, 319 (2016).
[35]K. Wood, A. Frölich, A. Paciaroni, M. Moulin, M. Härtlein, G. Zaccai, D. J. Tobias, and M. Weik, "Coincidence of dynamical transitions in a soluble protein and its hydration water: Direct measurements by neutron scattering and md simulations," J. Am. Chem. Soc. **130**, 4586–4587 (2008).
[36]A. Iorio, G. Camisasca, and P. Gallo, "Slow dynamics of hydration water and the trehalose dynamical transition," J. Mol. Liq. **282**, 617–625 (2019).
[37]J. L. F. Abascal and C. Vega, "A general purpose model for the condensed phases of water: TIP4P/2005," J. Chem. Phys. **123**, 234505 (2005).
[38]A. Srivastava, S. Malik, and A. Debnath, "Heterogeneity in structure and dynamics of water near bilayers using TIP3P and TIP4P/2005 water models," Chem. Phys. **525**, 110396 (2019).
[39]J. B. Klauda, R. M. Venable, J. A. Freites, J. W. O'Connor, D. J. Tobias, C. Mondragon-Ramirez, I. Vorobyov, A. D. MacKerell, and R. W. Pastor, "Update of the CHARMM all-atom additive force field for lipids: Validation on six lipid types," J. Phys. Chem. B **114**, 7830–7843 (2010).
[40]N. Kucerka, M.-P. Nieh, and J. Katsaras, "Fluid phase lipid areas and bilayer thicknesses of commonly used phosphatidylcholines as a function of temperature," Biochim. Biophys. Acta **1808**, 2761–2771 (2011).
[41]X. Zhuang, J. R. Makover, W. Im, and J. B. Klauda, "A systematic molecular dynamics simulation study of temperature dependent bilayer structural properties," Biochim. Biophys. Acta **1838**, 2520–2529 (2014).
[42]C. F. Lopez, S. O. Nielsen, M. L. Klein, and P. B. Moore, "Hydrogen bonding structure and dynamics of water at the dimyristoylphosphatidylcholine lipid bilayer surface from a molecular dynamics simulation," J. Phys. Chem. B **108**, 6603–6610 (2004).
[43]J. F. Nagle, R. Zhang, S. Tristram-Nagle, W. Sun, H. I. Petrache, and R. M. Suter, "X-ray structure determination of fully hydrated L alpha phase dipalmitoylphosphatidylcholine bilayers," Biophys. J. **70**, 1419–1431 (1996).
[44]H. Bekker, H. Berendsen, E. Dijkstra, S. Achterop, R. Vondrumen, D. van der Spoel, A. Sijbers, H. Keegstra, and M. Renardus, "GROMACS—A parallel computer for molecular-dynamics simulations," in *Physics computing' 92* (World Scientific, 1993), pp. 252–256.
[45]H. J. C. Berendsen, D. van der Spoel, and R. van Drunen, "GROMACS—A message-passing parallel molecular-dynamics implementation," Comput. Phys. Commun. **91**, 43–56 (1995).
[46]E. Lindahl, B. Hess, and D. van der Spoel, "GROMACS 3.0: A package for molecular simulation and trajectory analysis," Mol. Model. Annu. **7**, 306–317 (2001).
[47]D. Van Der Spoel, E. Lindahl, B. Hess, G. Groenhof, A. E. Mark, and H. J. C. Berendsen, "Gromacs: Fast, flexible, and free," J. Comput. Chem. **26**, 1701–1718 (2005).
[48]B. Hess, C. Kutzner, D. van der Spoel, and E. Lindahl, "GROMACS 4: Algorithms for highly efficient, load-balanced, and scalable molecular simulation," J. Chem. Theory Comput. **4**, 435–447 (2008).
[49]H. J. C. Berendsen, J. P. M. Postma, W. F. van Gunsteren, A. DiNola, and J. R. Haak, "Molecular dynamics with coupling to an external bath," J. Chem. Phys. **81**, 3684–3690 (1984).
[50]T. Darden, D. York, and L. Pedersen, "Particle mesh Ewald: An nlog(n) method for Ewald sums in large systems," J. Chem. Phys. **98**, 10089–10092 (1993).
[51]U. Essmann, L. Perera, M. L. Berkowitz, T. Darden, H. Lee, and L. G. Pedersen, "A smooth particle mesh Ewald method," J. Chem. Phys. **103**, 8577–8593 (1995).
[52]B. Hess, H. Bekker, H. J. C. Berendsen, and J. G. E. M. Fraaije, "LINCS: A linear constraint solver for molecular simulations," J. Comput. Chem. **18**, 1463–1472 (1997).
[53]P. Khakbaz and J. B. Klauda, "Investigation of phase transitions of saturated phosphocholine lipid bilayers via molecular dynamics simulations," Biochim. Biophys. Acta **1860**, 1489–1501 (2018).
[54]S. Tristram-Nagle, Y. Liu, J. Legleiter, and J. F. Nagle, "Structure of gel phase DMPC determined by x-ray diffraction," Biophys. J. **83**, 3324–3335 (2002).
[55]L. S. Vermeer, B. L. De Groot, V. Réat, A. Milon, and J. Czaplicki, "Acyl chain order parameter profiles in phospholipid bilayers: Computation from molecular dynamics simulations and comparison with ^{2}H NMR experiments," Eur. Biophys. J. **36**, 919–931 (2007).
[56]A. Debnath, F. M. Thakkar, P. K. Maiti, V. Kumaran, and K. G. Ayappa, "Laterally structured ripple and square phases with one and two dimensional thickness modulations in a model bilayer system," Soft Matter **10**, 7630–7637 (2014).
[57]A. Srivastava, S. Malik, S. Karmakar, and A. Debnath, "Dynamic coupling of a hydration layer to a fluid phospholipid membrane: Intermittency and multiple time-scale relaxations," Phys. Chem. Chem. Phys. **22**, 21158–21168 (2020).
[58]A. Debnath, B. Mukherjee, K. G. Ayappa, P. K. Maiti, and S.-T. Lin, "Entropy and dynamics of water in hydration layers of a bilayer," J. Chem. Phys. **133**, 174704 (2010).
[59]D. Mondal, S. Malik, P. Banerjee, N. Kundu, A. Debnath, and N. Sarkar, "Modulation of membrane fluidity to control interfacial water structure and dynamics in saturated and unsaturated phospholipid vesicles," Langmuir **36**, 12423–12434 (2020).
[60]A. Debnath, K. Ayappa, and P. K. Maiti, "Simulation of influence of bilayer melting on dynamics and thermodynamics of interfacial water," Phys. Rev. Lett. **110**, 018303 (2013).
[61]S. Gruenbaum and J. Skinner, "Vibrational spectroscopy of water in hydrated lipid multi-bilayers. I. Infrared spectra and ultrafast pump-probe observables," J. Chem. Phys. **135**, 08B616 (2011).

[62]Z. Zhang and M. L. Berkowitz, "Orientational dynamics of water in phospholipid bilayers with different hydration levels," J. Phys. Chem. B **113**, 7676–7680 (2009).
[63]A. Rahman, "Correlations in the motion of atoms in liquid argon," Phys. Rev. **136**, A405–A411 (1964).
[64]A. Arbe, P. Malo de Molina, F. Alvarez, B. Frick, and J. Colmenero, "Dielectric susceptibility of liquid water: Microscopic insights from coherent and incoherent neutron scattering," " Physical Review Letters **117**, 185501 (2016).
[65]A. Srivastava, S. Karmakar, and A. Debnath, "Quantification of spatio-temporal scales of dynamical heterogeneity of water near lipid membranes above supercooling," Soft Matter **15**, 9805–9815 (2019).
[66]F. W. Starr, J. F. Douglas, and S. Sastry, "The relationship of dynamical heterogeneity to the Adam-Gibbs and random first-order transition theories of glass formation," J. Chem. Phys. **138**, 12A541 (2013).
[67]C. Donati, J. F. Douglas, W. Kob, S. J. Plimpton, P. H. Poole, and S. C. Glotzer, "Stringlike cooperative motion in a supercooled liquid," Phys. Rev. Lett. **80**, 2338–2341 (1998).
[68]R. Das, C. Dasgupta, and S. Karmakar, "Time scales of Fickian diffusion and the lifetime of dynamic heterogeneity," Front. Phys. **8**, 210 (2020).
[69]L. V. Hove, "Correlations in space and time and born approximation scattering in systems of interacting particles," Phys. Rev. **95**, 249–262 (1954).
[70]W. K. Kegel and A. van Blaaderen, "Direct observation of dynamical heterogeneities in colloidal hard-sphere suspensions," Science **287**, 290–293 (2000).
[71]A. M. Puertas, M. Fuchs, and M. E. Cates, "Dynamical heterogeneities close to a colloidal gel," J. Chem. Phys. **121**, 2813–2822 (2004).
[72]P. Chaudhuri, L. Berthier, and W. Kob, "Universal nature of particle displacements close to glass and jamming transitions," Phys. Rev. Lett. **99**, 060604 (2007).
[73]S. Sengupta and S. Karmakar, "Distribution of diffusion constants and Stokes-Einstein violation in supercooled liquids," J. Chem. Phys. **140**, 224505 (2014).
[74]A. Jaiswal, T. Egami, and Y. Zhang, "Atomic-scale dynamics of a model glass-forming metallic liquid: Dynamical crossover, dynamical decoupling, and dynamical clustering," Phys. Rev. B **91**, 134204 (2015).
[75]G. Camisasca, M. De Marzio, D. Corradini, and P. Gallo, "Two structural relaxations in protein hydration water and their dynamic crossovers," J. Chem. Phys. **145**, 044503 (2016).
[76]J.-P. Hansen and I. R. McDonald, *Theory of Simple Liquids*, 4th ed., (Elsevier, 2013), pp. 363–401.
[77]M. Holz, S. R. Heil, and A. Sacco, "Temperature-dependent self-diffusion coefficients of water and six selected molecular liquids for calibration in accurate ^{1}H NMR PFG measurements," Phys. Chem. Chem. Phys. **2**, 4740–4742 (2000).
[78]H. Staley, E. Flenner, and G. Szamel, "Reduced strength and extent of dynamic heterogeneity in a strong glass former as compared to fragile glass formers," J. Chem. Phys. **143**, 244501 (2015).
[79]P. Viot, G. Tarjus, and D. Kivelson, "A heterogeneous picture of α relaxation for fragile supercooled liquids," J. Chem. Phys. **112**, 10368–10378 (2000).
[80]L. Xu, I. Ehrenberg, S. V. Buldyrev, and H. E. Stanley, "Relationship between the liquid–liquid phase transition and dynamic behaviour in the Jagla model," J. Phys.: Condens. Matter **18**, S2239 (2006).
[81]E. Rössler, "Indications for a change of diffusion mechanism in supercooled liquids," Phys. Rev. Lett. **65**, 1595 (1990).
[82]S.-H. Chen, F. Mallamace, C.-Y. Mou, M. Broccio, C. Corsaro, A. Faraone, and L. Liu, "The violation of the Stokes–Einstein relation in supercooled water," Proc. Natl. Acad. Sci. U. S. A. **103**, 12974–12978 (2006).
[83]F. Mallamace, C. Branca, C. Corsaro, N. Leone, J. Spooren, H. E. Stanley, and S.-H. Chen, "Dynamical crossover and breakdown of the Stokes Einstein relation in confined water and in methanol-diluted bulk water," J. Phys. Chem. B **114**, 1870–1878 (2010).
[84]E. Flenner and G. Szamel, "Dynamic heterogeneities above and below the mode-coupling temperature: Evidence of a dynamic crossover," J. Chem. Phys. **138**, 12A523 (2013).
[85]Y.-W. Li, Y.-L. Zhu, and Z.-Y. Sun, "Decoupling of relaxation and diffusion in random pinning glass-forming liquids," J. Chem. Phys. **142**, 124507 (2015).
[86]A. Luzar and D. Chandler, "Effect of environment on hydrogen bond dynamics in liquid water," Phys. Rev. Lett. **76**, 928 (1996).
[87]A. Chandra, "Effects of ion atmosphere on hydrogen-bond dynamics in aqueous electrolyte solutions," Phys. Rev. Lett. **85**, 768 (2000).
[88]D. van der Spoel, P. J. van Maaren, P. Larsson, and N. Tîmneanu, "Thermodynamics of hydrogen bonding in hydrophilic and hydrophobic media," J. Phys. Chem. B **110**, 4393–4398 (2006).
[89]A. Srivastava and A. Debnath, "Hydration dynamics of a lipid membrane: Hydrogen bond networks and lipid-lipid associations," J. Chem. Phys. **148**, 094901 (2018).
[90]A. Luzar and D. Chandler, "Hydrogen-bond kinetics in liquid water," Nature **379**, 55–57 (1996).
[91]A. Luzar, "Resolving the hydrogen bond dynamics conundrum," J. Chem. Phys. **113**, 10663–10675 (2000).
[92]C. Cammarota and G. Biroli, "Ideal glass transitions by random pinning," Proc. Natl. Acad. Sci. U. S. A. **109**, 8850–8855 (2012).
[93]W. Kob and D. Coslovich, "Nonlinear dynamic response of glass-forming liquids to random pinning," Phys. Rev. E **90**, 052305 (2014).
[94]N. Shafique, K. E. Kennedy, J. F. Douglas, and F. W. Starr, "Quantifying the heterogeneous dynamics of a simulated dipalmitoylphosphatidylcholine (DPPC) membrane," J. Phys. Chem. B **120**, 5172–5182 (2016).
[95]S. Dueby, V. Dubey, and S. Daschakraborty, "Decoupling of translational diffusion from the viscosity of supercooled water: Role of translational jump diffusion," J. Phys. Chem. B **123**, 7178–7189 (2019).
[96]N. Jan, "Large lattice random site percolation," Physica A **266**, 72–75 (1999).
[97]L. B. Pártay, P. Jedlovszky, I. Brovchenko, and A. Oleinikova, "Percolation transition in supercritical water: A Monte Carlo simulation study," J. Phys. Chem. B **111**, 7603–7609 (2007).
[98]S. Roy, S. Banerjee, N. Biyani, B. Jana, and B. Bagchi, "Theoretical and computational analysis of static and dynamic anomalies in water- DMSO binary mixture at low DMSO concentrations," J. Phys. Chem. B **115**, 685–692 (2011).
[99]S. Roy and B. Bagchi, "Solvation dynamics of tryptophan in water dimethyl sulfoxide binary mixture: In search of molecular origin of composition dependent multiple anomalies," J. Chem. Phys. **139**, 034308 (2013).
[100]F. Martelli, J. Crain, and G. Franzese, "Network topology in water nanoconfined between phospholipid membranes," ACS Nano **14**, 8616–8623 (2020).
[101]S. Samatas, C. Calero, F. Martelli, and G. Franzese, *Biomembrane Simulations: Computational Studies of Biological Membranes*, edited by M. L. Berkowitz (CRC Press, 2019), pp. 69–88.